Confined Nucleation and Growth of Poly(ethylene oxide) on the Different Crystalline Morphology of Poly(butylene succinate) From a Miscible Blend

ARTICLE *in* MACROMOLECULES · OCTOBER 2013

Impact Factor: 5.8 · DOI: 10.1021/ma4015214

3 AUTHORS, INCLUDING:

Yongri Liang
Beijing Institute of Petrochemical Technology
46 PUBLICATIONS **409** CITATIONS

Macromolecules

Article

pubs.acs.org/Macromolecules

Confined Nucleation and Growth of Poly(ethylene oxide) on the Different Crystalline Morphology of Poly(butylene succinate) From a Miscible Blend

Zhiyuan He,[†,‡] Yongri Liang,[†,*] and Charles C. Han[†,*]

[†]State Key Laboratory of Polymer Physics and Chemistry, Joint Laboratory of Polymer Science and Materials, Beijing National Laboratory for Molecular Sciences, Institute of Chemistry, Chinese Academy of Sciences, Beijing 100190, P. R. China

[‡]University of Chinese Academy of Sciences, Beijing, 100049, P. R. China

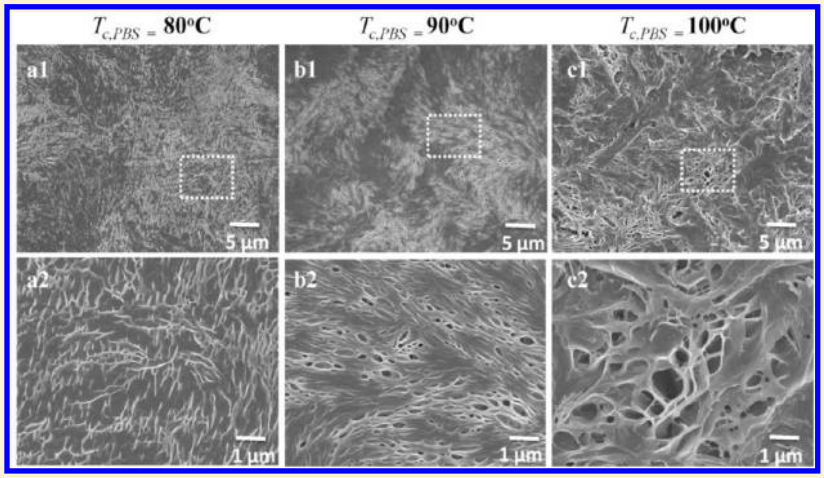

ABSTRACT: The confined and fractional crystallization behavior of poly(ethylene oxide)(PEO) in miscible poly(butylene succinate)(PBS)/PEO blends has been investigated. Both nucleation and growth of PEO crystals through the two-step crystallization process were significantly influenced by the morphology of pre-existed PBS spherulites. At the first crystallization step, the PEO component as diluents was segregated into different regions (interlamellar, interfibrillar and interspherulitic) of PBS crystals, which was dependent on the crystal growth rate of PBS and the diffusion coefficient of PEO. With the increase of crystallization temperatures of PBS ($T_{c,PBS}$), more and more PEO molecules were excluded out of the lamella stacks of PBS, and the segregations of PEO became larger and larger. Meantime, the connectivity between the adjacent PEO domains was reduced dramatically. At the second crystallization step, PEO crystallized subsequently within the existed frameworks of PBS spherulites formed at various $T_{c,PBS}$. On the one hand, the nucleation rate of PEO was determined by the total solid−liquid interfacial area between PBS crystals and PEO domains, which could significantly reduce the free energy barrier of nucleation embryos. As $T_{c,PBS}$ increased, the nucleation rate of PEO decreased with the decrease of PBS crystal surfaces which were around PEO domains. The fractional crystallization of PEO occurred when the nuclei formed at various supercoolings. On the other hand, the crystal growth rate of PEO was mostly influenced by the connectedness between the PEO domains. With the increase of $T_{c,PBS}$, the continuous phases of PEO were transformed into isolated domains. The crystal growth of PEO decreased gradually, due to the restrictions to the diffusion of PEO chains. PEO could only nucleate and grow inside each isolated domains, just forming tiny PEO crystals. It was found that the crystallization of PEO was dependent not only on the diffusion length of PEO, but also on the intrinsic morphological features of PBS spherulites.

1. INTRODUCTION

Recently, the crystalline/crystalline polymer blends have received much attention, which produced a wide variety of novel crystallization kinetics and superstructures.[1−4] In contrast with crystalline/amorphous polymer blends, the ultimate structures and morphologies are not only influenced by the miscibility and blend ratio, but also determined by the interplay between crystallizations of both crystalline components.[5−8] Though some progress has been achieved on the understanding of the crystallization behavior and related structure control of crystalline/crystalline polymer blends, however, it is still far from having a comprehensive and general picture on this subject; especially the crystallization of the lower-T_m component.

For the crystalline/crystalline polymer blends (A/B), when the difference in the melting points (T_m) of the two

Received: July 19, 2013
Revised: August 31, 2013
Published: October 3, 2013

components is large enough (>50 °C, $T_{m,A} > T_{m,B}$), both components are not crystallized simultaneously which normally resulted to a stepwise crystallization mechanism.[9] At the temperatures T such that $T_{m,A} > T > T_{m,B}$, the component A crystallizes first, and the blend represents as a crystalline/amorphous system. In this case, the component B acts as the diluents, which distributes in various crystalline spaces of component A (interlamelar, interfibrillar and interspherulitic regions).[10−13] The segregations of component B are dependent on the diffusion length, $\delta = D/G$, where D is the diffusion coefficient of the noncrystallizable species in the blend and G is the velocity of the crystallization front.[14,15] For temperatures $T < T_{m,B}$, the component B starts to crystallize inside the pre-existed spherulites of component A, then the blends get into the crystalline/crystalline state. A number of novel morphologies have been formed by the interplay between crystallizations of both components (A/B), such as side-by-side, interlocking, interpenetrating and interfiling spherulitic crystallizations.[9,16−18] In spite of the recent progress, an essential problem is still unsettled: How do the crystals of the lower-T_m component nucleate and grow inside the spatially limited regions of the pre-existed frameworks of the higher-T_m one.

Up to now, several studies have been focused on the confined and fractional crystallization of lower-T_m component upon stepwise crystallization process in the melt-miscible crystalline/crystalline polymer blends. It is found that the crystallization behaviors of the lower-T_m component are strongly influenced by the miscibility, blend composition and pre-existed crystalline morphology of the higher-T_m component. For example, Yang et al.[19,20] have investigated the effects of poly(vinylidene fluoride)(PVDF) on the crystallization kinetics, phase transition and morphology of polymorphic poly(butylene adipate)(PBA) in the miscible PVDF/PBA blend. It is noted that a small amount of PVDF in the solid state serves as the nucleating agent for PBA, while a large quantity of PVDF acting as the solidified matrix hinders the crystallization of PBA. Yan and co-workers[21] have investigated the morphology and phase segregation of PBA in the miscible poly(butylene succinate)(PBS)/PBA blend with optical and atomic force microscopy (POM/AFM) methods. It is found that the PBA melt segregate and distribute in different regions of PBS (interlamelar, interfibrillar and interspherulitic), depending on the compositions and crystallization temperature of PBS. Yan and co-workers[22,23] have also investigated the morphology and confined crystallization behavior of PBS in miscible PVDF/PBS blend. They show that the PBS crystal lamellae nucleate and grow confined in the matrix of PVDF spherulites, and the interconnectedness of the molten pockets within the PVDF spherulites determines the growth kinetics of PBS. Qiu et al.[24] have reported the overall crystallization kinetics of poly(butylene succinate-*co*-butylene adipate)(PBSA) in the miscible PBSA/PVDF blend. It is reported that the presence of the pre-existed PVDF crystals exerts two opposite effects on the crystallization of PBSA: enhancing the nucleation ability and reducing the crystal growth rates. Ikehara et al.[25] have reported the effect of lamellar growth direction and spherulitic boundary of PBS on the crystallization kinetics of PEO in the melt miscible PBS/PEO blend. They have found that the spherulite growth rate of PEO inside the PBS matrix (G_{PEO}) is greatly dependent on the crystallization temperature of PBS, and the PEO lamellae grow alongside the twisted lamella of PBS. He[8,26] and co-workers have studied the nanoconfined and fractional crystallization of PEO as a function of the crystallization temperature of PBS ($T_{c,PBS}$) in the miscible PBS/PEO blend. They suggested that the fractional crystallization of PEO was mainly determined by the positional distribution of PEO within the spherulites of PBS. The confined crystallization of PEO occurred when the PEO component was included in the interlamellar regions of PBS. Several excellent reviews have been given by Jungnickel[27] and Schultz.[14,28] As reviewed, a variety of works studied the crystallization of the lower-T_m component confined in the pre-existed crystal matrix of the higher-T_m one. However, only a few studies have been focused on the multiscale structures of the higher-T_m component and the nucleation and crystal growth of the lower-T_m component. Actually, owing to so many influencing factors, the mechanism of nucleation and crystal growth of the lower-T_m component in the crystalline/crystalline polymer blends has not been clear until now.

PBS and PEO are biodegradable and biocompatible semicrystalline polymers.[29,30] According to our previous study, the PBS/PEO blend has exhibited lower critical solution temperature (LCST) phase separation behavior at above the melting temperature of PBS.[31] It is found that the spatial distribution of PEO inside the PBS spherulites and the crystallization kinetics of PEO are both significantly influenced by the initial liquid−liquid phase morphology. In contrast to the previous study by using predemixed phase structures to control the final morphology, the miscible PBS/PEO blend (below the LCST) has been chosen as another model to disclose the effect of morphological features of PBS on the crystallization of PEO. In this work, the spatial distribution and diffusion length of PEO component within the PBS spherulites were dependent on the relative dynamic ratio of the crystal growth rate of PBS (G_{PBS}) to the diffusion rate of PEO (D_{PEO}). The fractional crystallization of PEO confined in the multiscale structures of PBS has also been investigated. It is found that the nucleation and crystal growth kinetics of PEO are not only dependent on the local concentration distribution of PEO driven by the crystallization of PBS, but also influenced significantly by the formation and connectivity of PEO segregations within the pre-existed PBS crystal scaffolds.

2. EXPERIMENTAL SECTION

2.1. Materials and Blend Sample Preparation. Poly(ethylene oxide) (PEO) with a number-average molecular weight of 2×10^4 g/mol was purchased from Sigma-Aldrich Company. Poly(butylene succinate)(PBS) was provided by Technical Institute of Physics and Chemistry, Chinese Academy of Sciences. The number-average molecular weight (M_n) of PBS was 8.6×10^4 g/mol, characterized by gel permeation chromatography (GPC) with eluant of chloroform. The glass transition temperatures of PBS and PEO were −30 °C and −60 °C, respectively. Samples of PBS/PEO (50:50 wt/wt) blend were prepared by solution casting using chloroform as a solvent. The polymer concentration was about 20 mg/mL. The mixed solutions were cast on the Petri dishes, and dried in a vacuum oven at 30 °C for 3 days. The melting temperature of PEO and PBS were measured to be about 64 and 114 °C, respectively, by differential scanning calorimeter (DSC, TA-Q2000) at a heating rate of 10 °C/min.

2.2. Miscibility and Thermal Programs. As shown in Figure 1, the phase diagram of PBS/PEO blend has been determined previously.[31] According to the phase diagram, PBS and PEO were completely miscible (below the LCST) in the melt. The temperature sequences upon step-crystallization based on the phase diagram were also indicated in Figure 1. The blends were first annealed at 140 °C for 5 min to erase thermal history, then crystallized at predetermined $T_{c,PBS}$ (80−100 °C) for 180 min, which was much higher than $T_{m,PEO}$. After the completion of PBS crystallization, the blends were further

dx.doi.org/10.1021/ma4015214 | Macromolecules 2013, 46, 8264−8274

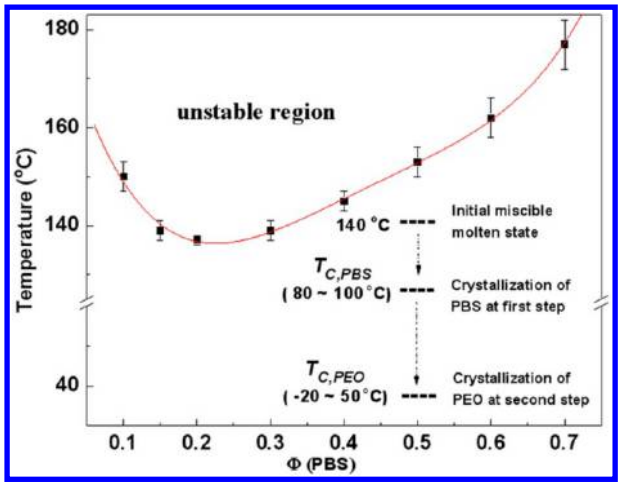

Figure 1. Phase diagram of PBS/PEO blend[31] and the step-crystallization temperature sequences used in this study.

quenched to the temperatures $T < T_{m,PEO}$, then the PEO component began to crystallize during isothermal and nonisothermal crystallization process.

2.3. Characterizations. *2.3.1. Scanning Electron Microscope.* Samples were examined by a scanning electron microscope (SEM, JEOL 6700F) for revealing the cross-section surface morphology of spherulites. Samples were etched by alcohol at 50 °C for 60 min to remove the component of PEO. Surfaces of samples were coated with platinum (Pt) before observation.

2.3.2. Optical Microscopy. Polarized optical microscopy (POM) and phase contrast optical microscopy (PCOM) images were observed by Olympus (BX51) optical microscope equipped with an Olympus camera (C-5050ZOOM). The sample temperatures were controlled by a Linkam (LTS 350) hot stage. The thickness of sample for optical microscopy measurements was about 20 μm. In the double-quench experiment, the PBS/PEO (50/50 wt/wt) blend sample was first crystallized at 100 °C for 20 min to obtain a semifinished crystalline structure on a hot stage. Then it was quickly transferred to another hot stage equipped with a camera, which was kept at 80 °C.

2.3.3. Differential Scanning Calorimeter. The nonisothermal crystallization processes of PEO component in the PBS/PEO (50:50 wt/wt) blends with different thermal histories of PBS were recorded by differential scanning calorimeter (DSC) (Q2000 TA Instruments). The temperature and heat flow were calibrated by pure Indium under nitrogen atmosphere before use.

2.3.4. Temperature-Resolved Synchrotron Wide-angle X-ray Scattering (WAXS) Measurement and Crystallinity. Temperature-resolved synchrotron wide-angle X-ray scattering measurement was carried out at the BL16B1 beamline in the Shanghai Synchrotron Radiation Facility (SSRF), China. The wavelength of the incident X-ray was 1.24 Å, and the sample to detector distance (SDD) was about 224 mm. The 2D WAXS data were collected by a Mar165 detector, and calibrated by silicon powder. The temperature of sample was controlled by an Instec HCS 301 hot stage.

The crystallinity was calculated from WAXS profiles, which was given by eq 1:

$$X_w = (A_{cry})/(A_{cry} + A_{amor}) \quad (1)$$

Here X_w is the mass crystallinity; A_{cry} and A_{amor} are areas of diffraction peaks contributed from crystalline and amorphous phases. Each of the crystalline peaks and amorphous scattering was fitted by Gaussian function, and the crystallinities were obtained by peak fitting method.[32] The total crystallinity $X_{w,t}$ (including both crystallinities of PBS and PEO component) and the crystallinity of PBS ($X_{w,PBS}$) were obtained at temperatures T ($T < T_{m,PEO}$) and temperatures T ($T_{m,PEO} < T < T_{m,PBS}$), respectively. It is estimated that the crystallinity of PEO can be calculated by $X_{w,PEO} = X_{w,t} - X_{w,PBS}$.

2.3.5. Temperature-Resolved Synchrotron Small-angle X-ray (SAXS) Scattering Measurement and SAXS Analysis. Temperature-resolved synchrotron small-angle X-ray scattering measurement was carried out at the 1W2A beamline in the Beijing Synchrotron Radiation Facility (BSRF), China. The wavelength of the incident X-ray was 1.54 Å, and the sample to detector distance (SDD) was about 2850 mm. The 2D SAXS data were recorded by time-resolved mode during cooling process (average exposure time was 60 s), and calibrated by silver behenate. The temperature of sample was also controlled by an Instec HCS 301 hot stage.

The structure parameters such as long period, thicknesses of crystalline and amorphous layers of PBS/PEO blend were obtained by normalized one-dimensional (1D) correlation function,[33] which defined as

$$\gamma(r) = \int_0^\infty I(q)q^2 \cos(qr)\, dq/Q \quad (2)$$

where $I(q)$ was the scattering intensity, q was the scattering vector defined as $q = (4\pi \sin\theta)/\lambda$ (2θ was the scattering angle), and r was the direction along the lamellar stack.

2.3.6. Time-Resolved Fourier Transform Infrared (FTIR) Spectroscopy. The time-resolved Fourier transform infrared (FTIR) spectra were recorded with 2 cm^{-1} of resolution and 32 times of scan by a Bruker TENSOR-27 FTIR spectrometer. The interval time for

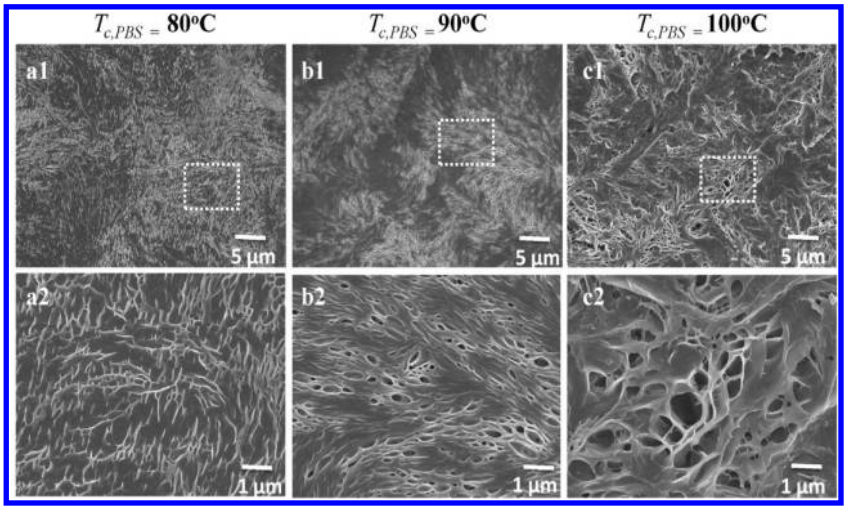

Figure 2. SEM cross-section images of PBS/PEO (50/50 wt/wt) blends following the crystallization of PBS at (a) 80, (b) 90, and (c) 100 °C. PEO was etched by alcohol before observation. Images 2 at the bottom were enlarged of the dashed boxes in images 1.

dx.doi.org/10.1021/ma4015214 | Macromolecules 2013, 46, 8264−8274

obtaining each spectrum was 5 s. The temperature of sample was controlled by an Instec HCS 301 hot stage which was set up in the beam path of infrared radiation.

3. RESULTS AND DISCUSSION

3.1. $T_{c,PBS}$-dependent Morphology of PBS in the PBS/PEO Blend. When PBS crystallized at temperatures above $T_{m,PEO}$, the PBS/PEO blends were treated as crystalline/amorphous system where PEO acted as an amorphous diluent. The PEO component segregated in different regions (interlamelar, interfibrillar and interspherulitic) of PBS spherulites, depending on the diffusion length $\delta = D_{PEO}/G_{PBS}$ (D_{PEO} is the diffusion coefficient of PEO and G_{PBS} is the radial growth rate of PBS spherulites). In order to observe the $T_{c,PBS}$-dependent spherulite morphological features of PBS and the segregations of PEO, the cross-section structures of PBS crystallized at various $T_{c,PBS}$ were detected by SEM as shown in Figure 2. The crystals of PEO were etched by alcohol before observation, revealing the underlying PBS scaffolds. For the sample ($T_{c,PBS}$ = 80 °C), the scaffolds of PBS were highly branched and quite open, exhibiting an irregular and interconnected network as shown in Figure 2a. As a result, the PEO segregations (etched portions) were not restricted by PBS frameworks and formed interconnected phases. When PBS crystallized at 90 °C as shown in Figure 2b, numerous tiny PEO-rich domains were formed and embedded into the interfibrillar regions of PBS spherulites. Meantime, the domains of PEO became less interconnected. As $T_{c,PBS}$ further increased to 100 °C, the PBS crystals exhibited cellular-like structures, in which the domains of PEO were isolated individually by the PBS bundles of fibril as shown in Figure 2c. According to the SEM results, with the increase of $T_{c,PBS}$, more and more portions of PEO component were aggregated into the interfibrillar regions of PBS spherulites, due to the increase of diffusion length. Meanwhile, as the PEO-rich domains become larger and larger, the connectivity between the adjacent PEO domains was reduced dramatically.

3.2. $T_{c,PBS}$-Dependent Nonisothermal Crystallization Behaviors of PEO in the PBS/PEO Blend. Following the crystallization of PBS component, PEO crystallized subsequently under different spatial confinement inside the spherulites of PBS at the second crystallization step. Figure 3 showed the DSC cooling curves of PBS/PEO blends and neat PEO with a cooling rate of 10 °C/min. Before the cooling process of PEO, PBS was crystallized at various $T_{c,PBS}$ for 180 min. According to the DSC data for all samples, the values of peak onset crystallization temperatures and corresponding crystallization enthalpies of PEO were all summarized in Table 1.

For polymer blends and block copolymer systems, crystallization upon cooling process could sometimes occur in several steps that were initiated at different supercoolings, which was known as fractional crystallization.[34,35] In this case, the fractional crystallizations of PEO were observed during the nonisothermal crystallization, which were similar to the results reported by He et al.[8,26] Almost all of the cooling curves of PBS/PEO blends exhibited two exothermic peaks: $T_{c,1}$ (small supercooling) and $T_{c,2}$ (large supercooling). The crystallization ability of neat PEO was strong, corresponding to the large crystallization enthalpy and high crystallization temperature. Compared with neat PEO, the crystallization kinetics of PEO in the PBS/PEO blends was suppressed. The crystallization temperature (see in Figure 3) as well as enthalpy (see in

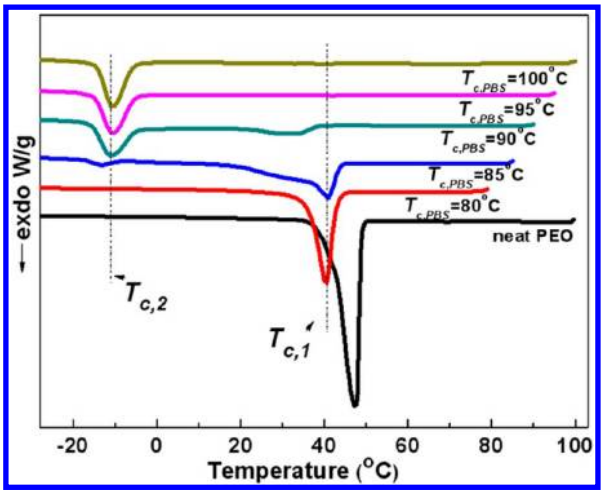

Figure 3. PEO crystallized with a cooling rate of 10 °C/min following the crystallization of PBS at various $T_{c,PBS}$ in the PBS/PEO (50/50 wt/wt) blend. The DSC cooling curve of neat PEO was also illustrated.

Table 1. Values of Peak Onset Crystallization Temperatures $T_{c1,onset}$ and $T_{c2,onset}$ and Corresponding Enthalpies (ΔH_c) of PEO during the Non-Isothermal Crystallization of PEO in PBS/PEO (50:50 wt/wt) Blends

sample ($T_{c,PBS}$, °C)	$T_{c1,onset}$ (°C)	$T_{c2,onset}$ (°C)	$\Delta H_{c,1}$ (J/g)	$\Delta H_{c,2}$ (J/g)	$\Delta H_{c,total}$ (J/g)
80	46.5	—	65.5	—	65.5
85	45.0	−2	52.2	2.6	54.8
90	39.5	−2	21.5	20.4	41.9
95	—	−2	—	38.5	38.5
100	—	−2	—	37.5	37.5
neat PEO	49.6	—	165.8	—	165.8

Table 1) decreased significantly with the increase of $T_{c,PBS}$. It is suggested that the crystallization of PEO was confined in the pre-existed scaffold of PBS spherulites. When $T_{c,PBS}$ was at 80 °C, the PEO cooling curve exhibited a single and sharp exothermal peak at about 40 °C. As $T_{c,PBS}$ further increased ($T_{c,PBS}$ = 80 and 90 °C), the crystallization peak of $T_{c,1}$ became much broader, and a weak crystallization peak of $T_{c,2}$ was discerned at about −10 °C. It is noted that the PBS crystals started to hinder the crystallization of PEO component. For the blends in which PBS crystallized at 95 and 100 °C, the crystallization of PEO could only occur at extremely lower temperatures, starting at about −10 °C and finally ending at around −18 °C. At the same time, ΔH_c of PEO decreased with the increase of $T_{c,PBS}$ as shown in Table 1. According to the DSC results, it is suggested that the fractional crystallizations of PEO corresponded to different nucleation and growth mechanisms in the pre-existed scaffold of PBS spherulites, depending significantly on the values of $T_{c,PBS}$.

The phenomenon of fractional crystallization usually has been observed in the immiscible polymer blends. It is reported that different groups of domains contained distinct active heterogeneities, and corresponded to different nucleation process (homogeneous nucleation, heterogeneous nucleation or self-nucleation).[36,37] As a result, the crystallization occurred at specific and independent supercooling. The confined and fractional crystallization were also reported in the macrophase separated block copolymer systems when the crystallizable block was the minor phase.[38,39] As far as we know, only a few

dx.doi.org/10.1021/ma4015214 | Macromolecules 2013, 46, 8264−8274

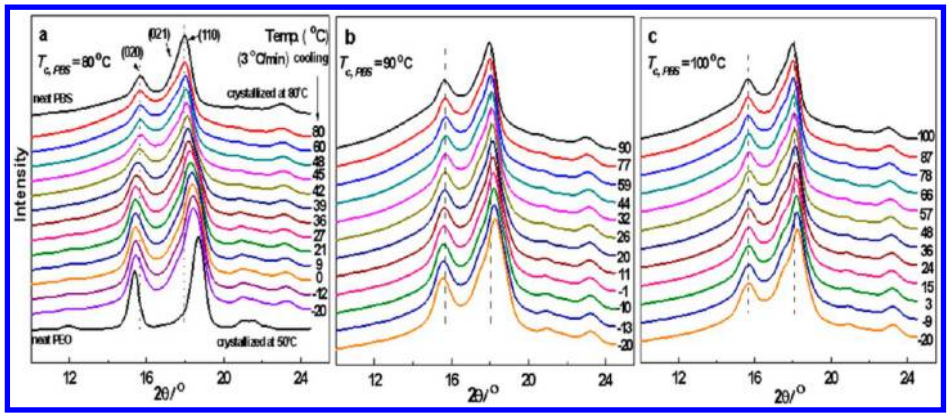

Figure 4. Temperature-resolved synchrotron WAXS profiles of PEO at different temperatures during cooling process with a cooling rate of 3 °C/min in the PBS/PEO (50:50 wt/wt) blends. PBS has been crystallized already at various $T_{c,PBS}$ before the cooling process. The WAXS profiles of crystallized neat PBS and PEO were also illustrated.

studies have reported the confined and fractional crystallizations in the melt-miscible polymer blends.[8,26,40]

In these melt-miscible PBS/PEO blend systems, it seems that the morphologies detected by SEM was contradict with the kinetics results of DSC. According to the usual understanding, the PEO component should crystallize faster or crystallize at higher temperatures upon cooling process when it had larger domain size in the blend crystallized at higher $T_{c,PBS}$, due to the smaller confinement effect. In fact, the results were contrary to the predictions. In order to clarify such complex phenomenon, both the nucleation and growth of PEO confined in multiple dimensions have been studied.

Figure 4 showed the temperature-resolved synchrotron WAXS profiles of PEO at different temperatures during the cooling process with a cooling rate of 3 °C/min. PBS has been crystallized already at various $T_{c,PBS}$ before the cooling process. When temperatures were above the $T_{m,PEO}$, no peaks corresponding to the crystalline phase of PEO diffraction were detected. All the blend samples have the same crystal structure (α-form crystal modification) of PBS, indicating that the existence of PEO and difference of $T_{c,PBS}$ did not change the PBS crystal form. According to the work of Ichikawa et al,[29] the diffraction peaks at 15.7°, 17.5°, and 18.2° corresponded to the (020), (021), and (110) planes of PBS α-form crystal. When temperatures further reduced, by comparing the WAXS curves of blends and corresponding pure polymers, the diffraction patterns just became a superposition of PBS and PEO after the subsequent crystallization of PEO. As described in the Experimental Section, each of the crystalline and amorphous diffraction peaks was fitted by Gaussian function, and the relative crystallinities X_w were obtained by peak fitting method.[32]

As shown in Figure 5, all measurements were done at 80 °C. Almost all of the shorter segments could crystallize when the samples ($T_{c,PBS}$ = 90 or 100 °C) were cooled down to 80 °C. As a result, the crystallinity of PBS remained constant (about 20%) with the change of $T_{c,PBS}$. It is suggested that the key factor which influenced the crystallization of PEO was not the PBS crystallinity. For the sample ($T_{c,PBS}$ = 80 °C), the PEO crystals nucleated immediately at 45 °C (denoted by the arrow), and then grew rapidly reaching saturation at about 20 to −10 °C. If the temperatures were lowered to below −10 °C, some new crystal nuclei of PEO formed again, which was not detected by DSC measurement, and the crystallinity increased slightly. For the sample ($T_{c,PBS}$ = 90 °C), the PEO nucleus could only form

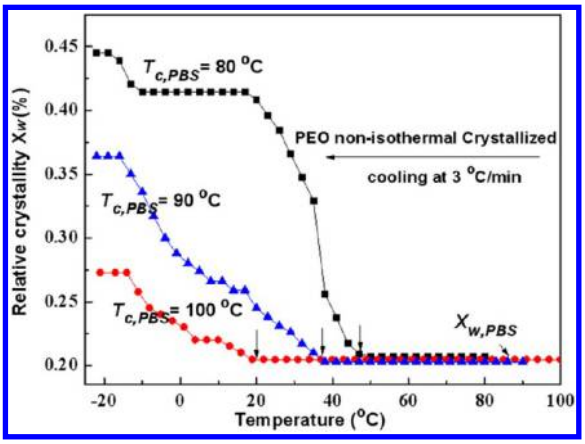

Figure 5. Relative crystallinity X_c during cooling process of PEO as a function of temperature.

in a higher degree of supercooling (below 36 °C). After that the crystals grew step by step until at −20 °C. As $T_{c,PBS}$ increased to 100 °C, the PEO component remained in the amorphous state until the temperature dropped to 20 °C. Then the crystals of PEO nucleated and grew continuously and slowly, and the growth stopped at about −20 °C. The crystal nuclei of PEO formed at increasingly larger supercooling, implying that the nucleation process was restricted as $T_{c,PBS}$ increased. Furthermore, the crystallinity of PEO ($X_{w,PEO} = X_{w,t} - X_{w,PBS}$) dropped significantly from 24% ($T_{c,PBS}$ = 80 °C) to7% ($T_{c,PBS}$ = 100 °C). It is suggested that the crystal growth of PEO was also restricted by the scaffolds of PBS, and the confinement was enhanced with the increase of $T_{c,PBS}$.

The nucleation and crystal growth of PEO within the PBS matrix were also observed by polarized optical microscopy (POM) as shown in Figure 6. Following the crystallization of PBS at different $T_{c,PBS}$ as shown in Figure 6a1−c1, the blends were further cooled to −30 °C with a cooling rate of 3 °C/min for the nonisothermal crystallization of PEO. In Figure 6a2−a4, the crystals of PEO nucleated quickly at about 40 °C within the PBS spherulites formed at 80 °C, and then grew rapidly to engulf the pre-existed PBS crystals. The spherical growth front of PEO could be observed clearly as denoted by the white circle in Figure 6a2, implying that the PEO chains were able to diffuse freely to the crystals growth front. When the $T_{c,PBS}$ was above 90 °C, it was impossible to observe the spherical growth of PEO, indicating that the crystal growth was under stricter

dx.doi.org/10.1021/ma4015214 | Macromolecules 2013, 46, 8264−8274

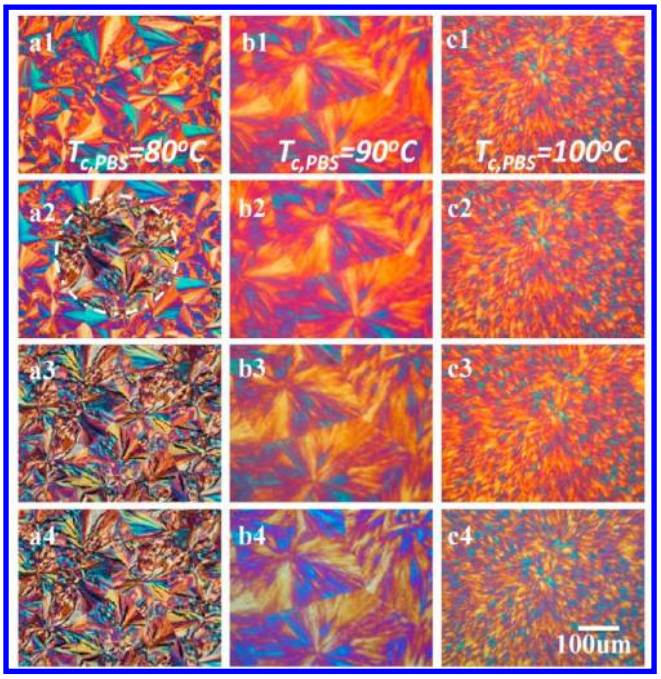

Figure 6. POM images of the PBS/PEO (50:50 wt/wt) blends at selected temperatures, (1) 80, (2) 40, (3) 10, and (4) −20 °C, during the cooling process with a cooling rate of 3 °C/min. PBS has been crystallized already at various $T_{c,PBS}$, (a) 80, (b) 90, and (c) 100 °C, before the cooling process.

restriction as $T_{c,PBS}$ increased. It was also implied that the diffusion of PEO chains between different PEO segregations started to be limited when $T_{c,PBS}$ was above 90 °C. Figure 6c1−c4 showed the crystallization of PEO inside the spherulites of PBS crystallized at 100 °C. The morphology of PBS spherulites was essentially the same before and after the crystallization of PEO.

3.3. $T_{c,PBS}$-Dependent Microstructure in the PBS/PEO (50/50 wt/wt) Blend. More detailed information on the crystallization morphology could not be observed by optical microscope due to the resolution limitation. In order to understand such complex fractional crystallization of PEO better, the lamella morphology and nanoscale structures of PBS/PEO blend were also determined by the temperature-resolved synchrotron SAXS technique. In the semicrystalline/amorphous state (measured at 80 °C), the structures at lamella level of PBS formed at different $T_{c,PBS}$ were investigated as shown in Figure 7a. The long period (L), amorphous layer thickness (l_a) and the average crystal thickness (l_c) (semicrystalline/amorphous state) estimated by 1D correlation function $\gamma(z)$ were displayed in Figure 7b,c. The position of the scattering peak shifted to a lower scattering angle and the characteristic long period (L) increased as $T_{c,PBS}$ increasing. The crystalline phase thickness (l_c) of PBS increased from 2.8 nm ($T_{c,PBS}$ = 80 °C) to 3.8 nm ($T_{c,PBS}$ = 100 °C). The thickness of amorphous layer (l_a) reduced from 6.3 to 5.7 nm. The volume change was calculated less than 10%. Meanwhile, the crystallinity of PBS in the PBS/PEO blends was independent of $T_{c,PBS}$. It is noted that the change of PBS/PEO composition in the amorphous phase before the second crystallization step was not significant. So the diffusion length and local distribution of PEO were not the main influential factors on the subsequent crystallization of PEO.

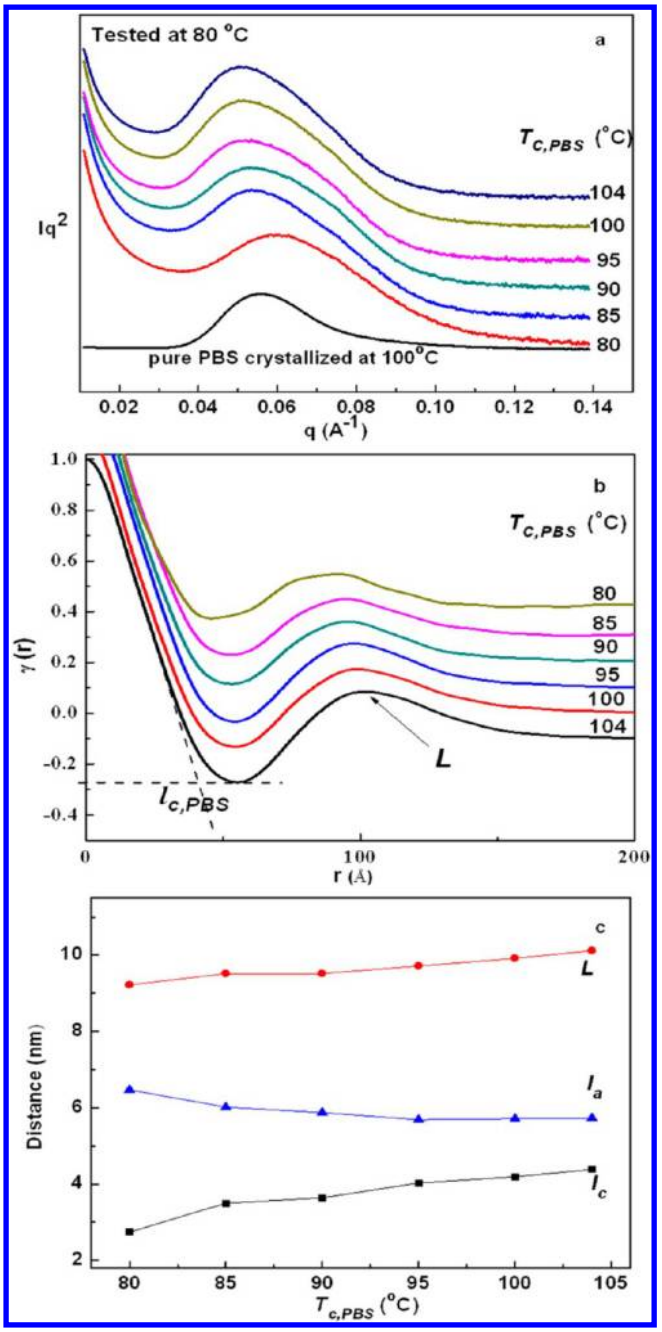

Figure 7. (a) Lorentz-corrected SAXS profiles; (b) normalized 1D correlation functions $\gamma(r)$; and (c) long period (L), amorphous layer thickness (l_a), and crystal thickness (l_c) of PBS/PEO blends obtained at 80 °C (in the semicrystalline/amorphous state) after the complete crystallization of PBS at various $T_{c,PBS}$.

As reviewed, He[8,26] have suggested that the fractional crystallization behavior of PEO was mainly determined by the local distribution of PEO within the different regions of PBS spherulites (interlamelar, interfibrillar and interspherulitic). The segregation of PEO (at higher $T_{c,PBS}$) in the interlamellar region of PBS resulted in the partial crystallization of PEO at a significantly large supercooling. The same explanations were also used in other crystalline/crystalline polymer blend systems.[19,21,40] According to our SAXS results, more and more PEO component was excluded out of the PBS lamella stacks with the increase of $T_{c,PBS}$, on the contrary, the

dx.doi.org/10.1021/ma4015214 | Macromolecules 2013, 46, 8264−8274

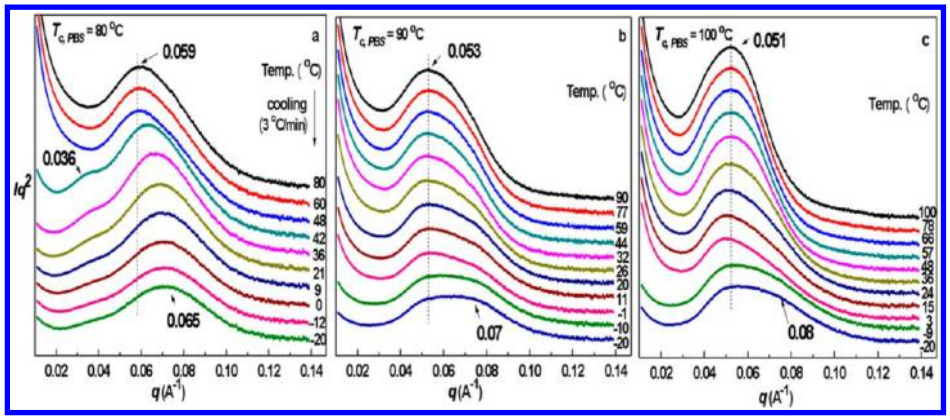

Figure 8. Temperature-resolved synchrotron SAXS profiles of PEO at different temperatures during cooling process with a cooling rate of 3 °C/min in the PBS/PEO (50:50 wt/wt) blends. PBS has been crystallized already at various $T_{c,PBS}$ before the cooling process.

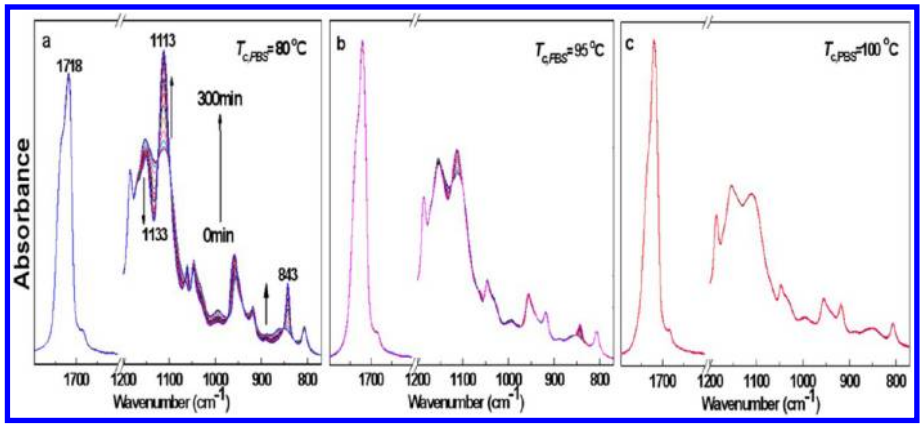

Figure 9. Time-dependent FTIR spectra in the wavenumber range of 1800−750 cm^{-1} during PEO crystallized at 50 °C following the crystallization of PBS at (a) 80, (b) 95, and (c) 100 °C in the PBS/PEO (50/50 wt/wt) blends.

crystallization of PEO was under much tougher confinement, which contradicted to the previous suggestion.

Following the crystallization of PBS, PEO crystallized during a cooling process subsequently within the crystals of PBS. The mechanisms of lamellar crystal growth of PEO from different nucleation process were investigated by the temperature-resolved synchrotron SAXS technique as shown in Figure 8. When $T_{c,PBS}$ was at 80 °C, PEO crystallized subsequently during a cooling process, a new scattering shoulder ($q \sim 0.036$ Å^{-1}) became visible in the low-q range at about 42 °C, related to the scattering of crystalline PEO. At the same time, the position of the main scattering peak of PBS ($q \sim 0.059$ Å^{-1}) shifted to higher-q region ($q \sim 0.065$ Å^{-1}) gradually as shown in Figure 8a. The crystals of PEO were unable to form inside the interlamellar region of PBS at such small supercooling (42 °C). So the decrease of long period (L) of PBS was attributed to the reduction of amorphous phase in the PBS lamellae. It is concluded that a portion of amorphous PEO was demixed and excluded out of the lamellar stacks of PBS during the crystallization of PEO. When PEO crystallized following the crystallization of PBS at above 90 °C as shown in Figure 8(b-c), the position of the scattering peak of PBS almost unchanged during the cooling process. It is suggested that the portion of PEO component which was confined in the interlamella regions of PBS, was unable to crystallize. In the sample ($T_{c,PBS}$ = 90 °C), a new scattering shoulder in the higher-q range ($q \sim 0.07$ Å^{-1}) was observed at about 10 °C, which was attributed to the crystallization of PEO. Because of the restriction and space limitation of PBS frameworks, PEO could only nucleate and grow in its isolated phase domains at larger supercooling, and forming thinner lamella. In the sample ($T_{c,PBS}$ = 100 °C), a weak and broad shoulder was observed in the much higher-q range ($q \sim 0.08$ Å^{-1}) until temperatures dropped below 0 °C, implying that much thinner lamella of PEO formed in such larger supercooling. According to the time-resolved SAXS results, PEO could hardly crystallize inside the interlamellar region of PBS. Owing to the increasingly confinement of PBS matrix, thinner lamella of PEO formed at larger supercooling in the interfibrillar region of PBS.

3.4. $T_{c,PBS}$-Dependent Isothermal Crystallization Kinetics of PEO in the PBS/PEO Blend. The detailed isothermal kinetics and minor changes of PEO crystallization were also investigated by time-resolved Fourier transform infrared (FTIR) spectroscopy. The infrared spectroscopy is sensitive to local molecular environment, which has been widely used to study the changes of interaction and structure of polymers in the crystallization process.[7] The isothermal crystallization kinetics of PEO at 50 °C was explored by time-resolved FTIR in the range of 1800−750 cm^{-1} following the completion of PBS crystallization at various crystallization temperatures ($T_{c,PBS}$ = 80, 85, 90, 95, and 100 °C). According to Figure 9, many bands of PBS and PEO component were highly overlapped. The band at 843 cm^{-1} assigned to the C−H rocking and C−O−C stretching vibrations was sensitive to the crystalline phase of PEO.[41] Thus, the band at 843 cm^{-1} was used as characteristic band to trace the crystallization process of

dx.doi.org/10.1021/ma4015214 | Macromolecules 2013, 46, 8264−8274

PEO. The band at 1718 cm^{-1}, which was coming from the C=O stretching vibration in crystalline state of PBS, was unchanged during the crystallization process of PEO. So the normalized peak intensity ratios of the 843 and 1718 cm^{-1} band (A_{843}/A_{1718}) as a function of the crystallization time at 50 °C were plotted to investigate the crystallization dynamics of PEO in Figure 10 and Table 2. The total crystallization rate (Figure 10a) as well as the induction time of crystallization (Figure 10b) changed significantly with the increase of $T_{c,PBS}$.

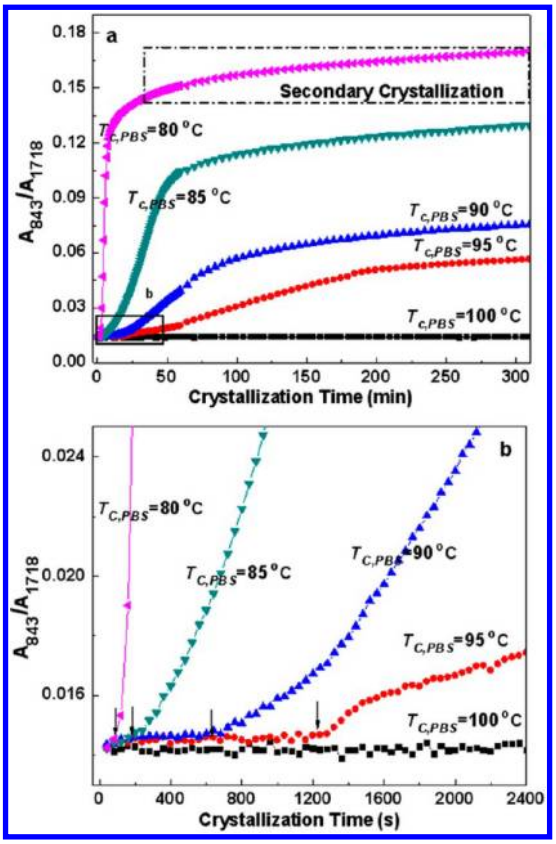

Figure 10. Normalized peak intensities ratio of the 843 and 1718 cm^{-1} band (A_{843}/A_{1718}) as a function of the crystallization time (a) 0−300 min and (b) 0−40 min at 50 °C calculated from the spectra in Figure 9. Part b was magnified image of square box of part a. The black arrows indicated the crystallization induction times.

Table 2. Values of Crystallization Half-Times ($t_{1/2}$) and Nucleation Induction Times of PEO

sample ($T_{c,PBS}$ °C)	80 °C	85 °C	90 °C	95 °C	100 °C
$t_{1/2}$ (min)	5	25	44	80	—
induction time (s)	40	120	680	1280	—

When $T_{c,PBS}$ was at 80 °C, the PEO crystals nucleated immediately and grew rapidly, and then the secondary crystallization process proceeded very slowly for several hours. As $T_{c,PBS}$ increased to 85 °C, the induction time of PEO crystallization increased from 40s to 120s. When PBS crystallized at 90 or 95 °C, it is obvious that the crystallization process proceeded more slowly. When $T_{c,PBS}$ further increased to 100 °C, the crystallization was almost prevented, and no obvious crystallization signal of PEO could be detected in the experiment, suggesting that the PEO chains needed to overcome severe restriction which has essentially prevented the nucleation. The induction time of PEO crystallization became much longer, implying that the nucleation rate of PEO decreased continuously as $T_{c,PBS}$ increased. According to the morphological changes detected by SEM, the phase domains of PEO within the PBS spherulites became larger and larger with the increase of $T_{c,PBS}$. It is noted that the nucleation of PEO crystals on or near the PBS crystal surfaces was the dominant factor.

Recently, Han and co-workers have reported a series of experiments on the polyolefin blend systems, and the mechanism of "concentration fluctuation-assisted crystallization" has been proposed.[42−44] It was described that the fluctuation could induce the chain segmental alignment to assist the primary nucleation of crystallization, especially at the interface of phase domains. According to the simulation results of Mitra and Muthukumar,[45] the formation of phase domains provided interfaces for heterogeneous nucleation, which could help decreasing the surface energy of crystallizing embryos and assisting the crystallization. Because of the interface-assisted crystallization theory, the heterogeneous nucleation on the interface could significantly reduce the free energy barrier of forming crystallizing embryos.[42−47] Since the nuclei were more likely to form at the interface, the faster heterogeneous nucleation was able to easily dominate the whole nucleation process. As a result, the nucleation rate of PEO was mostly dependent on the total solid−liquid interfacial area. When the domains of PEO became larger and larger, the relative interfacial area between PBS and PEO decreased sharply, dictating slow nucleation rate of PEO. At the same time, the crystal growth was also confined within the isolated domains restricted by the scaffolds of PBS crystals. As a result, the $t_{1/2}$ (crystallization half-time) increased a lot with the increase of $T_{c,PBS}$ as shown in Table 2. It is known that the overall kinetics results obtained by FTIR are statistically averaged for the whole sample, also including both nucleation and crystal growth rate. To obtain a better understanding of the crystal growth of PEO, some higher resolution microscopies have been also carried out.

Growth of PEO within Different Frameworks of PBS Spherulites. According to the kinetics results of time-resolved FTIR, both the nucleation and growth of PEO crystals were restricted within different frameworks of PBS spherulites. To better clarify the different effects of $T_{c,PBS}$ (80−100 °C) on the growth process of PEO inside the PBS spherulites, a double-quenched experiment was also carried out. The PBS/PEO (50/50 wt/wt) blend was first quenched from the melt to 100 °C for 20 min to obtain a semifinished crystalline structure, and then the sample was subsequently quenched to 80 °C for the completion of PBS crystallization. As shown in Figure 11 a1,b1, the two small spherulites marked by white circles were crystallized at 100 °C, and the surrounding crystals were formed subsequently at 80 °C during the second quench. The crystallization of PEO took place when the sample quenched to 50 °C as shown in Figure 11a2−a4 and (b2-b4). PEO started to nucleate somewhere out of the view field of the picture, and then grew rapidly to engulf the PBS crystals (formed at 80 °C) as denoted by the arrow in Figure 11a2−b2. With a first-order plate (λ = 530 nm) as compensator, the brightness of PBS spherulites decreased and the PEO crystallization exhibited subtractive interference to the birefringence of PBS spherulites. The PEO crystals continued to grow until the growth front encountered the spherulites of PBS crystallized at 100 °C as shown in Figure 11a3−b3. It is seen that PEO grew around the spherulites of PBS crystallized at 100 °C, like water flowing around stones, and was unable to penetrate into the spherulites.

dx.doi.org/10.1021/ma4015214 | Macromolecules 2013, 46, 8264−8274

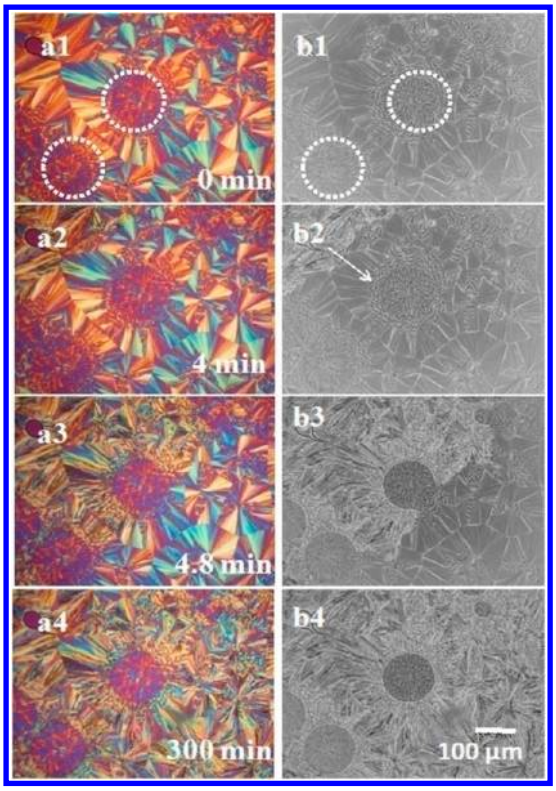

Figure 11. POM (a) and PCOM (b) images of PBS/PEO (50/50 wt/wt) blends quenched from the melt to 100 °C for 20 min, and then quenched to 80 °C for 180 min. PEO crystallized at 50 °C for (1) 0, (2) 4, (3) 4.8, and (4) 300 min.

The morphological feature and birefringence of PBS spherulites formed at 100 °C remained unchanged on the micrometer scale even though the sample stayed at 50 °C for 300 min.

In this set of experiments, it is obvious that PEO indeed nucleated and grew inside the spherulites of PBS formed at 80 °C instead of forming a double-layered structure where the two components crystallized separately. PEO grew isotropically and occupied the amorphous space inside the PBS spherulites. So the crystallization of PEO was restricted and strongly templated by the foregoing structure of PBS (formed at 80 °C). By contrast, PEO grew discretely and was unable to form regular growth boundary within the spherulites of PBS crystallized at 100 °C. Because of the disconnection of the isolated PEO domains dispersed in the PBS spherulites, the PEO chains could not diffuse efficiently to the growth front of spherulites.

The $T_{c,PBS}$-dependence of spherulitic growth rates of PEO (G_{PEO}) inside the PBS spherulites were also obtained by the spherulitic radius with crystallization time as shown in Figure 12. The value of the PEO spherulitic growth rate was not only dependent on the crystallization temperature of PEO, but also significantly influenced by the $T_{c,PBS}$. Compared with neat PEO, all the growth rate of PEO in the PBS/PEO blends was suppressed, since the confined effect in the scaffold of PBS spherulites. It is also observed that the spherulitic growth rate of PEO decreased with the increase of $T_{c,PBS}$ from 80 to 90 °C (see in Figure 12). It implied that the connectedness between the PEO domains was reduced. Therefore, the crystal growth of PEO became more and more limited, due to the restrictions to the diffusion of PEO chains. When the $T_{c,PBS}$ was above 90 °C, though the PEO component was able to nucleate (FTIR results), it was impossible to observe the spherulitic growth of PEO. The same results were also investigated in Figure 6.

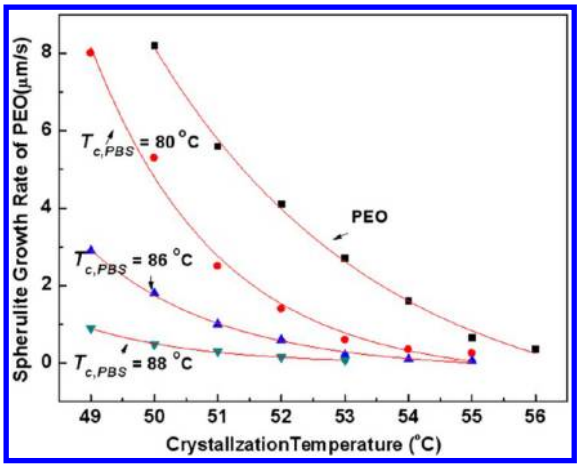

Figure 12. Dependence of the spherulitic growth rate of PEO on the $T_{c,PBS}$.

According to the secondary nucleation theory, the crystal growth rate was significantly determined by the ability of transporting the crystalline chains to the solid growth front or rejecting the amorphous chains out of the crystals. As $T_{c,PBS}$ increased, the segregations of PEO were divided and isolated inside the cellular-like frameworks of PBS, forming unconnected interfibrillar domains of PEO according to the SEM results. The limited spaces impeded the motion of PEO chains. As a result, the PEO growth rate decreased with the increase of $T_{c,PBS}$, due to the cause that the diffusion of PEO was confined. When the $T_{c,PBS}$ was above 90 °C, PEO might only nucleate and grow at large supercooling inside the confined spaces, forming tiny crystals which could not be detected by the optical microscope. The crystal growth of PEO was mostly influenced by the connectedness between the PEO domains inside the PBS spherulite: this interconnectedness effect was similar to that observed by Wang et al. for PVDF/PBS blends.[23] As reviewed, they found that the interconnectedness of the molten pockets within the PVDF spherulites determined the growth kinetics of PBS, and proposed the concept of "interconnectedness effect". There was some overlap of our views with that of Wang et al.;[23] however, the emphases were distinct.

4. CONCLUSIONS

In this work, the fractional crystallization behavior of PEO confined in various pre-existed PBS crystals formed at different $T_{c,PBS}$ have been investigated. In conclusion, the crystallization of PEO was dependent not only on the local concentration and segregations of PEO, but also on the intrinsic morphological features of PBS spherulites. It is found that both the crystal nucleation and growth of PEO were restricted on different length scales within the scaffolds of PBS, and the confinement effect was strengthened with the increase of $T_{c,PBS}$.

The crystal nucleation of PEO was significantly determined by the solid−liquid interface between PBS and PEO. The nucleation of PEO on or near the crystal surfaces of PBS could significantly reduce the free energy barrier of forming crystallizing embryos. With the increase of $T_{c,PBS}$, the phase domains of PEO within the PBS spherulites became larger and larger, and the total solid−liquid interfacial area decreased steeply. As a result, the nucleation rate of PEO decreased with the increase of $T_{c,PBS}$. The fractional crystallization of PEO

dx.doi.org/10.1021/ma4015214 | Macromolecules 2013, 46, 8264−8274

occurred due to the nuclei formed at various supercoolings, depending on the different effect of interface-assisted crystallization by PBS matrix.

The crystal growth of PEO was mostly influenced by the connectedness between the PEO domains. When $T_{c,PBS}$ was at 80 °C, the scaffolds of PBS were highly branched and quite open, resulting in an interconnected and continuous phases of PEO. Thus, the PEO chains were able to diffuse continuously to the crystal growth front, and the spherulitic growth of PEO within the PBS spherulites could be observed by optical microscope. With the increase of $T_{c,PBS}$, the connectedness between the PEO domains was reduced dramatically. The crystal growth of PEO became more and more limited, due to the restrictions to the diffusion of PEO chains. PEO could only nucleate and grow inside each isolated domains, just forming tiny PEO crystals. Hence, the regular growth front could not be observed at the microscopic scale.

Because of the crossover effect of pre-existed PBS crystals on both crystal nucleation and growth of PEO, the overall crystallization kinetics and crystallinity of PEO decreased sharply with the increase of $T_{c,PBS}$. It is noted that the confined and fractional crystallization of PEO was not determined by the nanoconfined crystallization between PBS interlamellar, but influenced by the confined crystal nucleation and growth of PEO on different length scales. Our results have provided some new insights into the interplay between crystallizations of both crystalline components in the melt-miscible crystalline/crystalline polymer blends.

AUTHOR INFORMATION

Corresponding Authors

*(C.C.H.) E-mail: c.c.han@iccas.ac.cn.

*(Y.L.) E-mail: liangyr@iccas.ac.cn. Telephone: +86 10 82618089. Fax: +86 10 62521519.

Notes

The authors declare no competing financial interest.

ACKNOWLEDGMENTS

This research work was supported by National Natural Science Foundation of China (No. 50930003 and Young scientist fund, No. 21004070) and the project sponsored by the Scientific Research Foundation for the Returned Overseas Chinese Scholars, State Education Ministry ([2010], No.1561). The synchrotron WAXS experiments were supported by Shanghai Synchrotron Radiation Facility (SSRF), China. The synchrotron SAXS experiments were supported by Beijing Synchrotron Radiation Facility (BSRF), China.

REFERENCES

(1) Penning, J. P.; Manley, R.; St, J. *Macromolecules* **1996**, *29*, 77−83.

(2) Qiu, Z.; Ikehara, T.; Nishi, T. *Macromolecules* **2002**, *35*, 8251−8254.

(3) Jungnickel, B. J. *Lect. Notes Phys.* **2003**, *606*, 208−237.

(4) Qiu, Z.; Ikehara, T.; Nishi, T. *Polymer* **2003**, *44*, 2799−2806.

(5) Nurkhamidah, S.; Woo, E. M. *Macromolecules* **2012**, *45*, 3094−3103.

(6) Chiu, H. J.; Chen, H. L.; Lin, J. S. *Polymer* **2001**, *42*, 5749−5754.

(7) Zhang, J.; Sato, H.; Furukawa, T.; Tsuji, H.; Noda, I.; Ozaki, Y. *J. Phys. Chem.* **2006**, *110*, 24463−24471.

(8) He, Y.; Zhu, B.; Kai, W.; Inoue, Y. *Macromolecules* **2004**, *37*, 3337−3345.

(9) Liu, J. P.; Qiu, Z. B.; Jungnickel, B. J. *J. Polym. Sci., Part B: Polym. Phys.* **2005**, *43*, 287−295.

(10) Chiu, H. J.; Chen, H. L.; Lin, T. L.; Lin, J. S. *Macromolecules* **1999**, *32*, 4969−4974.

(11) Chiu, H. J.; Lin, H. H.; Lin, J. S. *Macromolecules* **2000**, *33*, 4856−4860.

(12) Chuang, W. T.; Jeng, U. S.; Sheu, H. S.; Hong, P. D. *Macromol. Res.* **2006**, *14*, 45−51.

(13) Chuang, W. T.; Jeng, U. S.; Hong, P. D.; Sheu, H. S.; Lai, Y. H.; Shih, K. S. *Polymer* **2007**, *48*, 2919−2927.

(14) Schultz, J. M. *Macromolecules* **2012**, *45*, 6299−6323.

(15) Liu, L. Z.; Chu, B.; Penning, J. P.; Manley, R.; St, J. *Macromolecules* **1997**, *30*, 4398−4404.

(16) Yang, J.; Pan, P.; Hua, L.; Xie, Y.; Dong, T.; Zhu, B.; Inoue, Y.; Feng, X. *Polymer* **2011**, *52*, 3460−3468.

(17) Hernandez, M. C.; Laredo, E.; Bello, A.; Carrizales, P.; Marcano, L.; Balsamo, V.; Grimau, M.; Muller, A. J. *Macromolecules* **2002**, *35*, 7301−7313.

(18) Woo, E. M.; Hsieh, Y. T.; Chen, W. T.; Kuo, N. T.; Wang, L. Y. *J. Polym. Sci., Part B: Polym. Phys.* **2010**, *48*, 1135−1147.

(19) Yang, J.; Pan, P.; Hua, L.; Zhu, B.; Dong, T.; Inoue, Y. *Macromolecules* **2010**, *43*, 8610−8618.

(20) Yang, J.; Pan, P.; Hua, L.; Feng, X.; Yue, J.; Ge, Y.; Inoue, Y. *J. Polym. Sci., Part B: Polym. Phys.* **2012**, *116*, 1265−1272.

(21) Wang, H.; Gan, Z.; Schultz, J. M.; Yan, S. *Polymer* **2009**, *49*, 2342−2353.

(22) Wang, T.; Li, H.; Wang, F.; Schultz, J. M.; Yan, S. *Polym. Chem.* **2011**, *2*, 1688−1698.

(23) Wang, T.; Li, H.; Wang, F.; Yan, S.; Schultz, J. M. *J. Phys. Chem. B* **2011**, *115*, 7814−7822.

(24) Qiu, Z.; Yan, C.; Lu, J.; Yang, W. *Macromolecules* **2007**, *40*, 5047−5053.

(25) Ikehara, T.; Kurihara, H.; Kataoka, T. *J. Polym. Sci., Part B: Polym. Phys.* **2009**, *47*, 539−547.

(26) He, Y.; Zhu, B.; Kai, W.; Inoue, Y. *Macromolecules* **2004**, *37*, 8050−8056.

(27) Liu, J.; Jungnickel, B. J. *J. Polym. Sci., Part B: Polym. Phys.* **2007**, *45*, 1917−1931.

(28) Schultz, J. M. *Front. Chem. China* **2010**, *5*, 262−276.

(29) Ichikawa, Y.; Kondo, H.; Igarashi, Y.; Noguchi, K.; Okuyama, K.; Washiyama, J. *Polymer* **2000**, *41*, 4719−4727.

(30) Qiu, Z.; Ikehara, T.; Nishi, T. *Polymer* **2003**, *44*, 2799−2806.

(31) He, Z.; Liang, Y.; Wang, P.; Han, C. C. *Polymer* **2013**, *54*, 2355−2363.

(32) Yang, J.; Liang, Y.; Luo, J.; Zhao, C.; Han, C. C. *Macromolecules* **2012**, *45*, 4254−4261.

(33) Strobl, G. R.; Schneider, M. *J. Polym. Sci., Part B: Polym. Phys.* **1980**, *18*, 1343−1359.

(34) *Polymer Blends Handbook*; Utracki, L. A., Ed.; Springer: Heidelberg, Germany, 2003; Vols. *1* and *2*.

(35) Michell, R. M.; Lorenzo, A. T.; Muller, A. J.; Lin, M. C.; Chen, H. L.; Blaszczyk-Lezak, I.; Martin, J.; Mijangos, C. *Macromolecules* **2012**, *45*, 1517−1528.

(36) Arnal, M. L.; Matos, M. E.; Morales, R. A.; Santana, O. O.; Muller, A. J. *Macromol. Chem. Phys.* **1998**, *199*, 2275−2288.

(37) Arnal, M. L.; Muller, A. J. *Macromol. Chem. Phys.* **1999**, *200*, 2559−2576.

(38) Opitz, R.; Lambreva, D. L.; de Jeu, W. H. *Macromolecules* **2002**, *35*, 6930−6936.

(39) Muller, A. J.; Balsamol, V.; Arnal, M. L.; Jakob, T.; Schmalz, H.; Abetz, V. *Macromolecules* **2002**, *35*, 3048−3058.

(40) Pan, P.; Zhao, L.; Yang, J.; Inoue, Y. *Macromol. Mater. Eng.* **2013**, *298*, 201−209.

(41) Zhu, S.; Chen, J.; Li, H.; Cao, Y. *Appl. Surf. Sci.* **2013**, *264*, 500−506.

(42) Zhang, X. H.; Wang, Z. G.; Muthukumar, M.; Han, C. C. *Macromol. Rapid Commun.* **2005**, *26*, 1285−1288.

(43) Zhang, X. H.; Wang, Z. G.; Zhang, R. Y.; Han, C. C. *Macromolecules* **2006**, *39*, 9285−9290.

(44) Shi, W. C.; Chen, F. H.; Zhang, Y.; Han, C. C. *ACS Macro Lett.* **2012**, *1*, 1086−1089.

(45) Mitra, M. K.; Muthukumar, M. *J. Chem. Phys.* **2010**, *132*, 184908.
(46) Muthukumar, M. *Adv. Chem. Phys.* **2004**, *128*, 1−63.
(47) Muthukumar, M. *Philos. Trans. R. Soc. London, A* **2003**, *361*, 539.